




Article

On-Chip Bandstop to Bandpass Reconfigurable Filters Using Semiconductor Distributed Doped Areas (ScDDAs)

Rozenn Allanic ^{1,*}, Fabien Le Borgne ¹, Hassan Bouazzaoui ¹, Denis Le Berre ¹, Cédric Quendo ¹, Douglas Silva De Vasconcellos ², Virginie Grimal ², Damien Valente ² and Jérôme Billoué ²

¹ Laboratoire des Sciences et Techniques de l'Information, de la Communication et de la Connaissance (Lab-STICC), Université de Brest, 29238 Brest, France

² Laboratoire GREMAN, Université de Tours, 37071 Tours, France

* Correspondence: rozenn.allanic@univ-brest.fr

Abstract: This paper presents two novel on-chip bandstop to bandpass reconfigurable filters in C and X bands. Designed on a silicon substrate, filter reconfigurability is achieved using semiconductor-distributed doped areas (ScDDAs), such as an N⁺PP⁺ junction integrated into the substrate. The active element is therefore co-designed with the passive parts, allowing flexibility in ScDDA size and position. This flexibility offers advantages in terms of integration, ease of manufacture, and performance. The synthesis was developed in the OFF-state in order to match with the well-known one in the ON-state. As proof of concept, 5 GHz and 10 GHz filters were built. The simulated and measured results showed good agreement in both bandpass and bandstop configurations.



Citation: Allanic, R.; Le Borgne, F.; Bouazzaoui, H.; Le Berre, D.; Quendo, C.; Silva De Vasconcellos, D.; Grimal, V.; Valente, D.; Billoué, J. On-Chip Bandstop to Bandpass Reconfigurable Filters Using Semiconductor Distributed Doped Areas (ScDDAs). *Electronics* **2022**, *11*, 3420. <https://doi.org/10.3390/electronics11203420>

Academic Editor:
Enrique Romero-Cadaval

Received: 29 August 2022

Accepted: 17 October 2022

Published: 21 October 2022

Publisher's Note: MDPI stays neutral with regard to jurisdictional claims in published maps and institutional affiliations.



Copyright: © 2022 by the authors. Licensee MDPI, Basel, Switzerland. This article is an open access article distributed under the terms and conditions of the Creative Commons Attribution (CC BY) license (<https://creativecommons.org/licenses/by/4.0/>).

Keywords: active filter; bandpass filter; bandstop filter; BPF; BSF; co-design; on-chip; PIN diode; reconfigurable; ScDDA; silicon devices; switchable; tunable filter

1. Introduction

Reconfigurability has been one of the major concerns for designers of microwave components and systems in recent years. Indeed, with the multiplication of smart objects, driven by the increasing number of users, devices need to be flexible. Reconfigurability allows system integration with a reduced number of components, combined with a reduced cost and improved performance.

Reconfigurable planar microwave filters are often associated with RF MEMS [1–3] or PIN diodes [4,5]. These active elements allow the frequency, bandwidth, or both, to vary. Moreover, reconfigurability can be achieved by switching a filter from bandstop to bandpass [6–10].

However, additional active components induce parasitic effects at the connections with the passive parts, e.g., because of a size difference. These parasitic effects result in losses and/or frequency shifts, design constraints, and a limitation in the frequency rise.

Furthermore, on-chip systems appear to offer a solution for integration. Some studies have shown that it is possible to design a reconfigurable on-chip filter [11–13] using GaAs technology.

Moreover, on silicon technology, on-chip reconfigurable resonators were demonstrated in [14]. Thanks to the co-design method flexibility, multiple working states were performed with a single DC command. This was done using integrated active elements, such as semiconductor-distributed doped areas (ScDDAs) with different junction sizes. With a particular doping shape, a tunable resonator can continuously vary its resonant frequency by 50% [15]. Still on a silicon substrate, an on-chip reconfigurable bandpass filter (BPF) achieved bandwidth tunability [16] with a wide bandwidth choice. Finally, frequency reconfigurable filters have been co-designed with the same method using interdigital and dual behavior resonator topologies [17,18].

Considering classical approaches, previous studies show that it is possible to obtain a compact bandstop filter (BSF) using a coupled line and an interference transmission line [19] and a reconfigurable bandstop to bandpass filter using a coupled line and switchable transmission lines to short-circuit the resonators [20].

In this paper, we present two novel on-chip bandstop to bandpass reconfigurable filters which allow the use of only one integrated active element instead of two PIN diodes in classical PCB technology. Moreover, this approach leads to a greatly reduced parasitic problem related to the reported component and can be applied at quite high frequencies. Section 2 presents the idea of the reconfigurable filter and both syntheses, i.e., bandpass and bandstop. Then, Section 3 deals with the first demonstrator, a 5 GHz reconfigurable filter. The simulated and measured results are presented and analyzed. Once the concept was validated at 5 GHz, Section 4 proposes a 10 GHz reconfigurable filter demonstrator to show flexibility in terms of frequency and bandwidth. Finally, in Section 5, we compare the results with state-of-the-art to show the interest of the reconfigurable on-chip filters, notably at 10 GHz.

2. Synthesis

2.1. Reconfigurable Filter

The idea of this work is to design a reconfigurable filter with active elements allowing the commutation from a bandpass to a bandstop filter. When the switches are short-circuited, the filter is a bandpass filter formed by two short-circuited resonators and a coupled line. When the switches are opened, the filter is a bandstop filter formed by a transmission line in parallel with the coupled line. Figure 1 presents the topology of the filter.

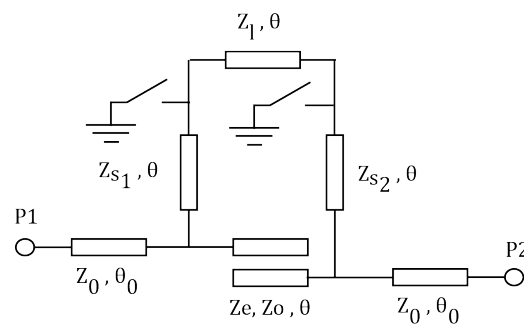


Figure 1. Ideal reconfigurable filter.

2.2. Bandpass Filter

The bandpass filter synthesis starts from that of the lowpass filter synthesis in [21]. Figure 2a illustrates an example of a 4th-order filter.

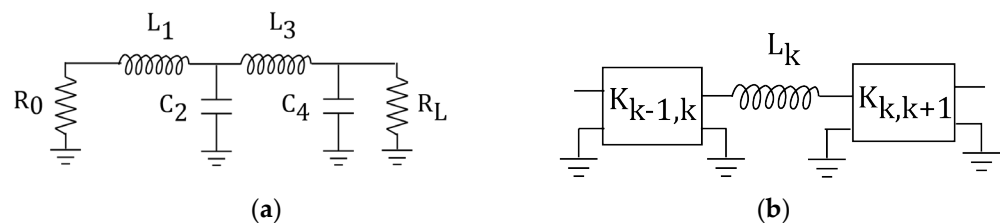


Figure 2. (a) Lowpass filter. (b) Modified prototype using impedance inverters.

The inductances and the capacitances can be evaluated from (1) and (2) with the Chebyshev coefficients listed in Table 1.

$$L_i = \frac{R_0 g_k}{\omega_0} \quad \text{with } i \text{ even} \tag{1}$$

$$C_i = \frac{g_k}{R_0 \omega_0} \quad \text{with } i \text{ odd} \tag{2}$$

Table 1. Chebyshev coefficients of a 4th-order filter for a 0.01 dB ripple.

n	g ₀	g ₁	g ₂	g ₃	g ₄	g ₅	ω' ₁
4	1	0.7128	1.2003	1.3212	0.6476	1.1007	1

Then, a transformation (Figure 2b) of the capacitance is applied to obtain inverters and inductances in series, where the values are determined with (3) to (6). The impedances of the inverters are chosen to be equal to 50 Ω.

$$K_{0,1} = \sqrt{\frac{R_0 L_1}{g_0 g_1}} \tag{3}$$

$$K_{k,k+1} = \sqrt{\frac{L_k L_{k+1}}{g_k g_{k+1}}}, \quad K_{n,n+1} = \sqrt{\frac{R_L L_n}{g_n g_{n+1}}} \tag{4}$$

$$K_{0,1} = K_{k,k+1} = K_{n,n+1} = 50 \Omega \tag{5}$$

$$L_1 = \frac{K_{k-1,k}^2 g_{k-1} g_k}{R_g}, \quad L_{k+1} = \frac{K_{k,k+1}^2 g_k g_{k+1}}{L_k} \tag{6}$$

Each inductance is then transformed into a series inductor with a capacitance, as shown in Figure 3. Their values can be calculated with (7).

$$L'_k = \frac{\beta L_k}{\omega_0}, \quad C'_k = \frac{1}{\beta L_k \omega_0}, \quad \beta = \frac{f_c}{\Delta f} \tag{7}$$

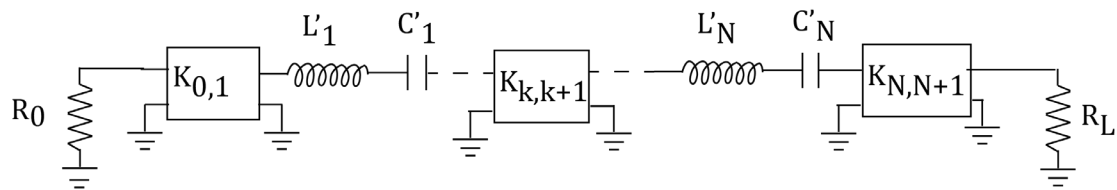


Figure 3. Bandpass filter prototype.

The next step is to convert the 4th-order bandpass filter with inductances, capacitances, and impedance inverters to transmission lines with short-circuited resonators and coupled lines, as shown in Figure 4. To do this, two inductances and capacitances with an impedance inverter are transformed into a transmission line with two serial open-circuited stubs to end up with a coupled transmission line, as illustrated in Figure 5.

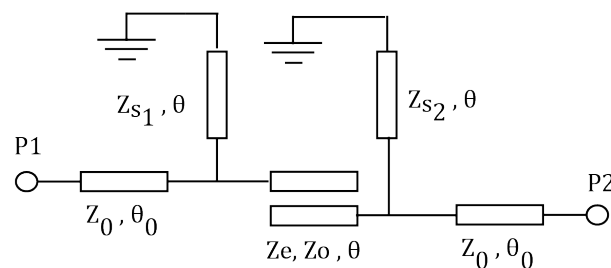


Figure 4. Bandpass filter.

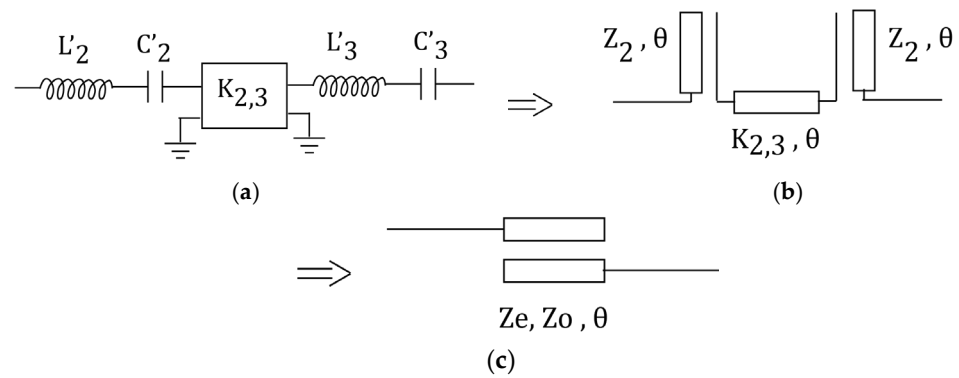


Figure 5. Coupled line transformation. (a) Inductances and capacitances with impedance inverter. (b) Transmission line with two serial open-circuited stubs. (c) A coupled transmission line.

This is done by applying Richards’ transformation with (8) and (9). Then, to symmetrize the coupled lines, we consider $Z_2 = Z_3$.

$$Z_2 = L'_2 \times \frac{\pi\omega_0}{4}, \quad Z_3 = L'_3 \times \frac{\pi\omega_0}{4} \tag{8}$$

$$Z_o = Z_2, \quad Z_e = 2K_{2,3} + Z_2 \tag{9}$$

Once the coupled line elements are determined, the short-circuited resonator impedance can be calculated using Richards’ transformation, converting inductance and capacitance in series with inverter impedance into an inductance in parallel with capacitance and then in short-circuited stub (as shown in Figure 6).

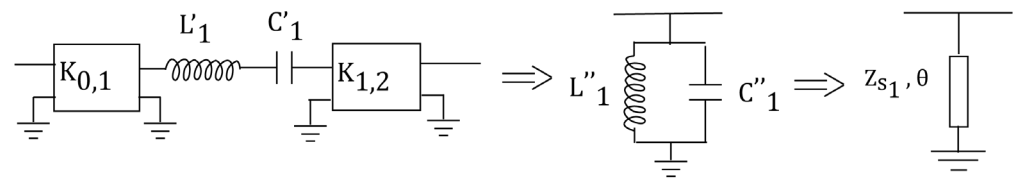


Figure 6. Short-circuited stub transformation.

This can be done using (10) to (14). The same operation can be performed for both short-circuited resonators. It should be noted that Z_1 is the impedance resulting from the connection in series of the inductance L'_1 and the capacitor C'_1 .

$$Z_1 = \frac{1 - C'_1 L'_1 \omega^2}{jC'_1 \omega} \tag{10}$$

$$Z_1 = K_{0,1} K_{1,2} \left(jC''_1 \omega + \frac{1}{jL''_1 \omega} \right) \tag{11}$$

$$L''_1 = C'_1 K_{0,1} K_{1,2} \tag{12}$$

$$Z_{s1} = C'_1 \times K_{0,1} \times K_{1,2} \times \frac{\pi\omega_0}{4} \tag{13}$$

$$Z_{s2} = C'_4 \times K_{3,4} \times K_{4,5} \times \frac{\pi\omega_0}{4} \tag{14}$$

2.3. Bandstop Filter

At this stage, we synthesized the bandpass filter, and we propose in this section a new synthesis of the bandstop filter in order to match with the bandpass one. The topology of the bandstop filter is presented in Figure 7a, and can be simplified with two parallel matrices, as shown in Figure 7b.

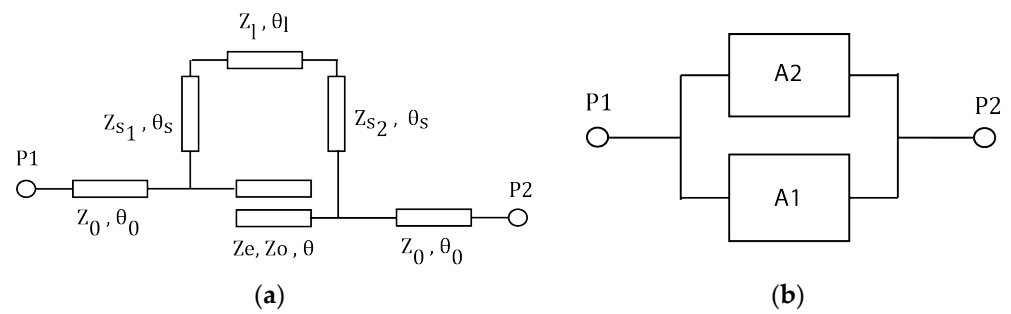


Figure 7. (a) Ideal bandstop filter. (b) Matrix representation of the bandstop filter.

The first matrix A_1 , in (15), represents the coupled line where it was considered that $\theta_s = 90^\circ$ at the resonant frequency, and the second matrix A_2 in (16) is for the three transmission lines with a total length including the two lengths of the resonator and the additional one between both of them.

The total admittance is the addition of the two admittance matrices, as shown in (17).

$$[A_1] = \begin{bmatrix} \cos \theta + \frac{z_2 \cos \theta}{k_{23}} & \frac{\cos^2 \theta}{j \sin \theta} \left(2 \times z_2 + \frac{z_3^2}{k_{23}} \right) + j k_{23} \sin \theta \\ \frac{j}{k_{23}} \sin \theta & \frac{z_2 \cos \theta}{k_{23}} + \cos \theta \end{bmatrix} \quad (15)$$

$$[A_2] = \begin{bmatrix} -\cos \theta_1 & -\frac{j Z_{s1} Z_{s2}}{Z_1} \sin \theta_1 \\ \frac{-j Z_1}{Z_{s1} Z_{s2}} \sin \theta_1 & -\cos \theta_1 \end{bmatrix} \quad (16)$$

$$[Y_{tot}] = [Y_1] + [Y_2] \quad (17)$$

If the transmission S_{21} is null at the central frequency, this implies Y_{21} is null, which makes it possible to obtain the impedance of the additional line between the two resonators, as in (18).

$$Z_1 = \frac{Z_{s1} Z_{s2}}{K_{2,3}} \quad (18)$$

3. Reconfigurable Filter at 5 GHz

3.1. Concept and Simulations

Based on this synthesis, a fourth-order reconfigurable filter at 5 GHz with a 3.5 GHz bandwidth, i.e., 70% bandwidth, was synthesized, and the calculated parameters are listed in Table 2 and the final theoretical impedances in Table 3. This filter was designed and built on a 675 μm HR-Si substrate, i.e., with a resistivity of 2500 $\Omega \cdot \text{cm}$ (Figure 8), which is a p-type substrate doped with boron.

Table 2. Parameter values of the 5 GHz filter different elements from the synthesis.

L_1	L_2	L_3	L_4	L'_2	L'_3	$K_{0,1}$	$K_{2,3}$	Z_2	Z_3
35.6	60	66	40.5	2.73×10^{-9}	3×10^{-9}	50	50	67	74

Table 3. Impedance values of the 5 GHz filter different elements.

Z_a	Z_o	Z_e	Z_{s1}	Z_{s2}	Z_1
50 Ω	74 Ω	174 Ω	39 Ω	41 Ω	31 Ω

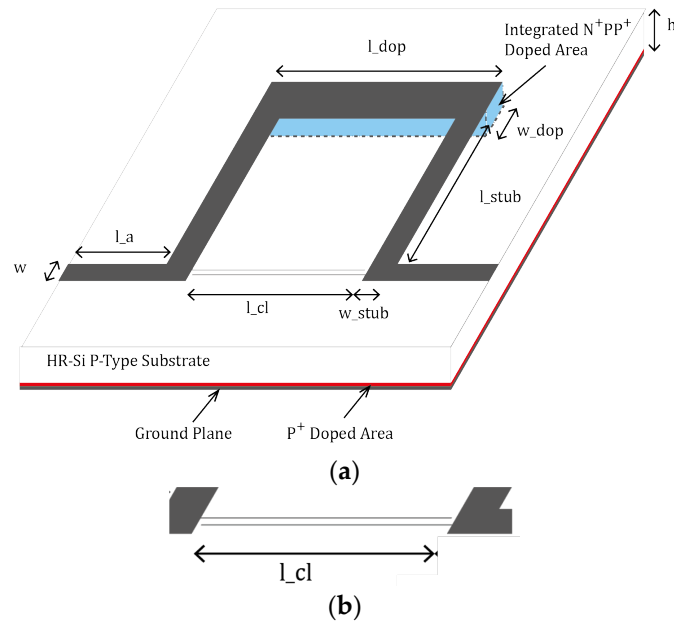


Figure 8. (a) Three-dimensional design of the 5 GHz reconfigurable filter. (b) Zoom on the coupled lines.

The reconfigurability is achieved using an integrated N^+PP^+ junction. Figure 9 shows the integrated N^+PP^+ junction and its models in the OFF- and ON-states.

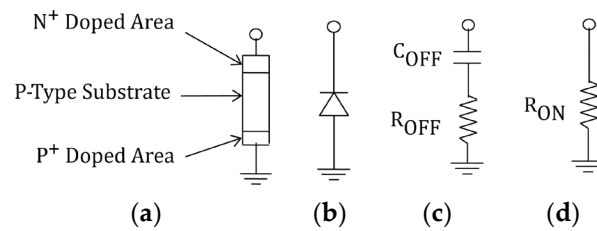


Figure 9. (a) Integrated junctions. (b) Diode. (c) OFF-state ideal model. (d) ON-state ideal model.

The OFF-state is considered without junction bias. The junction model is a high-value resistor R_{OFF} in series with a capacitor C_{OFF} . The ON-state is considered with a forward bias voltage of the junction, and its model is a low resistor R_{ON} . Therefore, the longer the dimensions of the ScDDAs, the lower the resistor value in the ON-state, and the lower the losses. That is why the whole length of θ_1 is doped. The dimensions of the optimized filter, taking into account the discontinuities, are summarized in Table 4.

Table 4. Dimensions of the 5 GHz reconfigurable filter.

Access	$l_a = 3.18$ mm	$w = 0.54$ mm
Coupled line	$l_{cl} = 5.34$ mm	$w_{cl} = 0.02$ mm $s = 0.14$ mm
Stub ₁	$l_{stub1} = 4.57$ mm	$w_{stub1} = 0.9$ mm
Stub ₂	$l_{stub2} = 4.57$ mm	$w_{stub2} = 0.82$ mm
Doped area	$l_{dop} = 7.26$ mm	$w_{dop} = 1.15$ mm

l_x = length of each part. w_x = length of each part.

In the simulation, the junction is approximated as a rectangular parallelepiped under the doped area. Its height is the same as the substrate thickness, and its surface is equal to

the N⁺ doped surface. The loss tangent is calculated at each frequency depending on the resistivity values using (19) [22].

$$\tan \delta = \frac{1}{\rho \omega \epsilon_0 \epsilon_r} + 0.0018 \tag{19}$$

In the OFF-state, the resistivity is taken as 2500 Ω.cm (given between 500 Ω.cm and 10 kΩ.cm by the manufacturer) in the whole substrate (Figure 10a). In the ON-state, the integrated active junction is simulated with a low resistivity of 0.5 Ω.cm (Figure 10b).

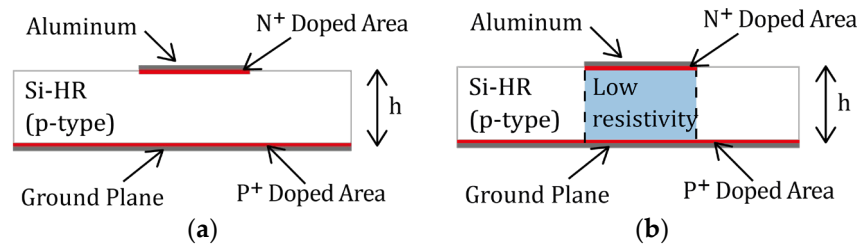


Figure 10. (a) OFF-state modeling. (b) ON-state modeling.

The simulated results obtained using the electromagnetic software HFSS™ are presented in Figure 11 in both states.

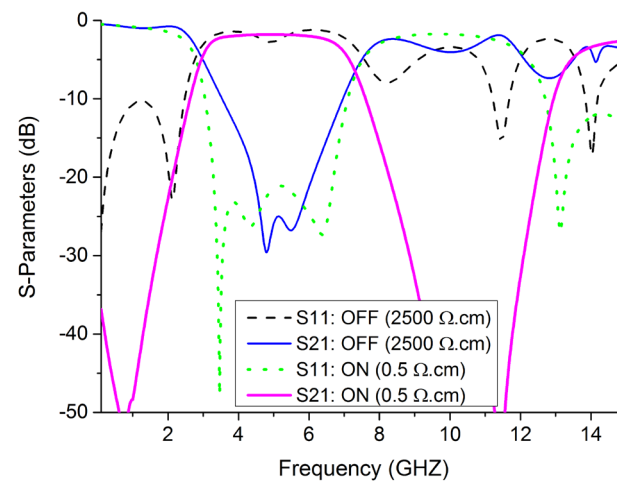


Figure 11. Simulated results in both states.

In the OFF-state, the filter is a 5 GHz bandstop filter with a 3.5 GHz bandstop (from 3.5 GHz to 7 GHz) and a transmission level below −10 dB. At the center frequency, the transmission level is lower than −25 dB. In the ON-state, the 5 GHz bandpass filter has a 3 dB bandwidth of 4 GHz from 3 GHz to 7 GHz. The insertion loss at the center frequency is equal to 1.8 dB. Using (20) from [21], the unloaded *Q*_u-factor is 12, with an 80% fractional bandwidth *w* in the ON-state.

$$IL(dB) = \frac{4.343 * n}{w * Q_u} \tag{20}$$

3.2. Measurement

This filter was manufactured using only two masks: one for the N⁺ doping and the other for the top face metallization. The two doped areas (N⁺ on the top face and P⁺ on the bottom face) were each 3 μm in depth with a doping concentration at the surface of 3 × 10¹⁹ atoms/cm³ using a sol-gel solution. Around 3 μm of aluminum was deposited on both faces.

A photograph of the 5 GHz filter is shown in Figure 12. This filter was placed in a measurement cell and measured using a vector network analyzer (VNA) (ZVA 67 GHz from R&S®).

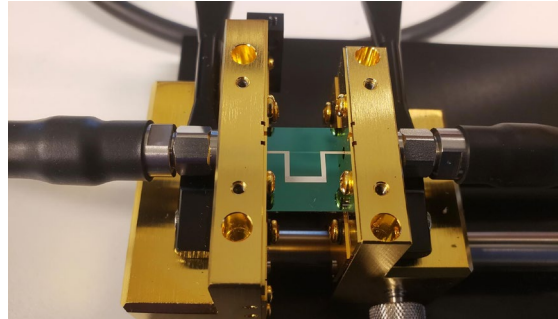


Figure 12. Photograph of the device under test.

The bias voltage allowing filter commutation was ensured by an external source and two bias tees in order to protect the VNA. A short open load through calibration was performed to remove the losses of the cables, but the losses of the filter included the losses of the measurement cell. The measured results are given in Figure 13.

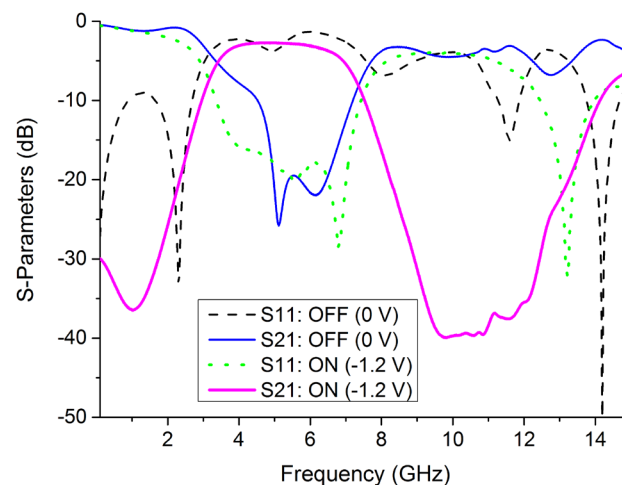


Figure 13. Measured results of the S-parameters in both states.

In the OFF-state, without bias voltage, the stopband filter had a transmission level lower than -16 dB at the center frequency. The -10 dB bandwidth was achieved from 4.5 GHz to 7.2 GHz. In the ON-state, a bias voltage of -1.2 V was applied to the junction. The measured insertion loss was 2.7 dB, and the -3 dB bandwidth was from 3.3 GHz to 7 GHz. Moreover, taking into account all measured losses, including those of the measurement cell, the measured Qu-factor was evaluated as 8.6, with a 75% fractional bandwidth w in the ON-state.

A comparison between the simulated and the measured results is given in Figure 14 for the OFF- and ON-states.

There was good agreement between the simulated and the measured results. The slight differences were due to uncertainties concerning the concentration and thickness of the doping layers.

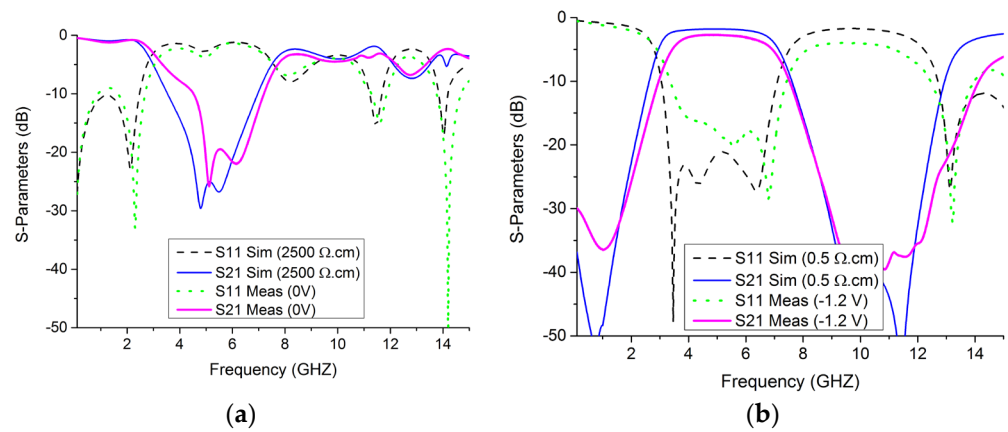


Figure 14. Comparison of the simulated and the measured results: (a) in the OFF-state; (b) in the ON-state.

4. The 10 GHz Reconfigurable Filter

4.1. Design and Simulations

To demonstrate the interest of the approach at higher frequencies, a fourth-order reconfigurable filter at 10 GHz with a 10 GHz bandwidth, i.e., a 100% bandwidth, was also synthesized, and the calculated parameters are listed in Table 5. The final theoretical impedances are listed in Table 6. Another bandwidth was chosen to show flexibility as another proof of concept. The design is presented in Figure 15.

Table 5. Parameter values of the 10 GHz filter different elements from the synthesis.

L_1	L_2	L_3	L_4	L'_2	L'_3	$K_{0,1}$	$K_{2,3}$	Z_2	Z_3
35.6	60	66	33.7	9.6×10^{-10}	1.05×10^{-9}	50	50	47	52

Table 6. Impedance values of the 10 GHz filter different elements.

Z_a	Z_o	Z_e	Z_{s1}	Z_{s2}	Z_1
50 Ω	52 Ω	152 Ω	55 Ω	58 Ω	64 Ω

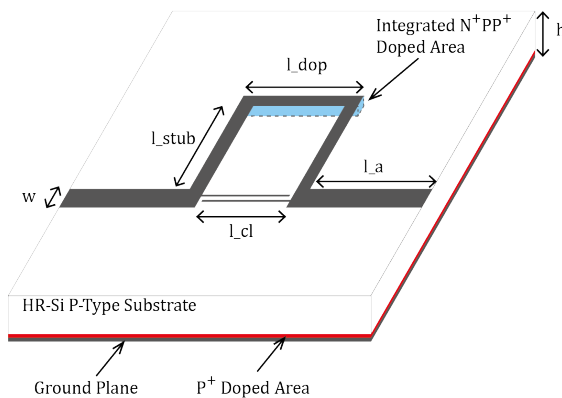


Figure 15. The 3D design of the 10 GHz reconfigurable filter.

After optimization, its dimensions are summarized in Table 7, and the simulated results are given in Figure 16.

Table 7. Dimensions of the 10 GHz reconfigurable filter.

Access	$l_a = 3.61 \text{ mm}$	$w = 0.55 \text{ mm}$
Coupled line	$l_{cl} = 2.6 \text{ mm}$	$w_{cl} = 0.05 \text{ mm}$ $s = 0.1 \text{ mm}$
Stub ₁	$l_{stub1} = 2.4 \text{ mm}$	$w_{stub1} = 0.46 \text{ mm}$
Stub ₂	$l_{stub2} = 2.4 \text{ mm}$	$w_{stub2} = 0.39 \text{ mm}$
Doped area	$l_{dop} = 3.55 \text{ mm}$	$w_{dop} = 0.3 \text{ mm}$

l_x = length of each part. w_x = length of each part.

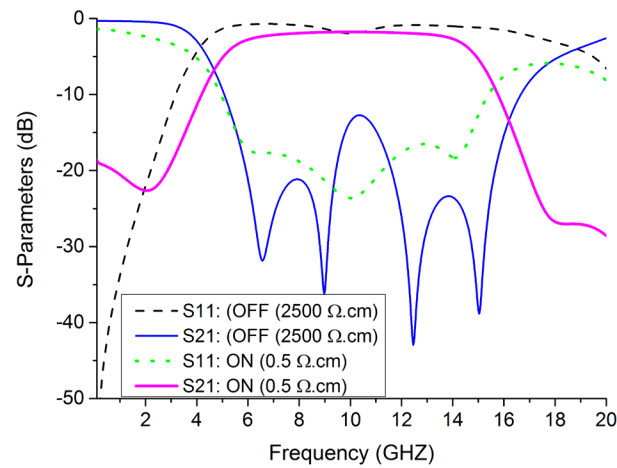


Figure 16. Simulated results of the 10 GHz filter in both states.

In the OFF-state, the transmission level was below -13 dB in the whole bandstop frequency range (i.e., from 5 GHz to 16.7 GHz). In the ON-state, the insertion loss was lower than 1.8 dB , and the reflection coefficient was higher than 16 dB , with a -3 dB bandwidth from 5.1 GHz to 14.9 GHz. In this case, the simulated Qu-factor was 9.85, and the fractional bandwidth w was 98% in the ON-state.

4.2. Measurement

This filter was manufactured on the same wafer as the 5 GHz filter, with the same process flow. A photograph of the filter is shown in Figure 17, and the measured results are given in Figure 18.

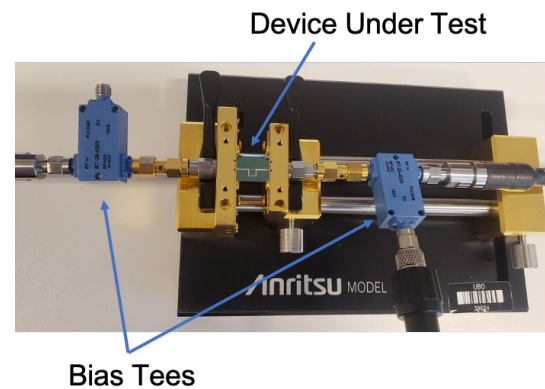


Figure 17. Photograph of the 10 GHz filter under test.

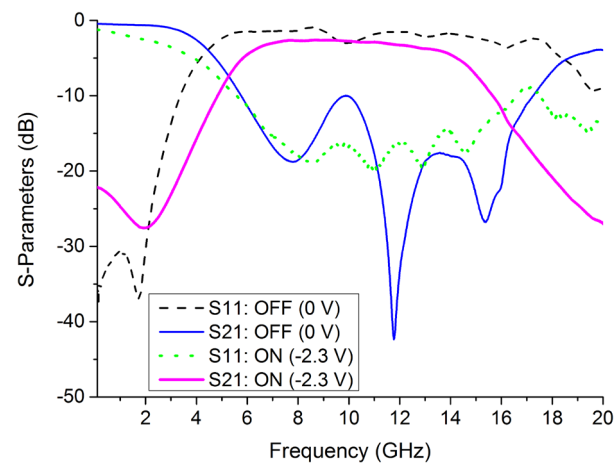


Figure 18. Measured results of the 10 GHz filter in both states.

In the OFF-state, with a 0 V bias voltage, the transmission level was below -10 dB across the whole frequency bandstop from 5.7 GHz to 17.3 GHz. In the ON-state, with a 2.3 V bias voltage, the insertion loss was 2.6 dB at the center frequency, and a return loss above 16 dB was observed. The -3 dB bandwidth was from 5.65 GHz to 14.5 GHz. Here, with the whole measured losses of the filter and the measurement cell, the measured Qu-factor was evaluated as 7.5, with an 89% fractional bandwidth w in the ON-state. A good agreement was found between the simulated and the measured results in the OFF- and ON-states, as shown in Figure 19.

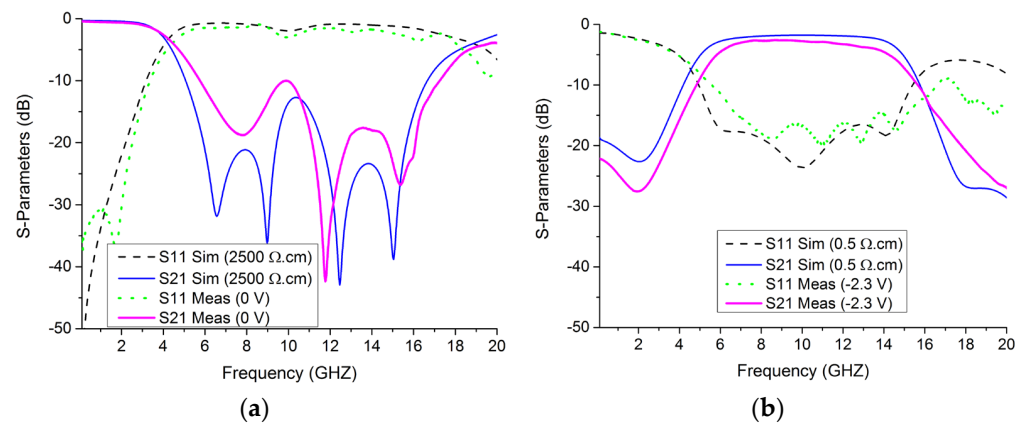


Figure 19. Comparison between the simulated and the measured results of the 10 GHz filter. (a) In the OFF-state. (b) In the ON-state.

5. Discussion

To our knowledge, few studies have dealt with a reconfigurable bandpass to bandstop filters in C and X bands, as proposed in this paper. Table 8 presents a comparison between the two presented filters and reconfigurable bandpass to bandstop filters found in the literature. The filters proposed here are competitive with these others. Improvement could be obtained with compactness techniques and an increase in the doping quantity to minimize losses. However, on PCBs, the use of classical PIN diodes induces parasitic effects linked to the interconnections between the active and passive parts. Therefore, we should have used two diodes instead of one doped area and one more DC line to bias the middle point between the two classical diodes. Thanks to the distributed area, the losses can be minimized compared to the use of classical PIN diodes at 10 GHz.

Table 8. Comparison with previous reconfigurable bandpass to bandstop filters and this work.

Ref.	Frequency	Reconfigurability Method	States-Number	IL in Bandpass Mode	In-Band Rejection in Bandstop Mode	Electrical Dimensions
[6]	0.9–1.6 GHz	4 trimmer caps and 4 pin diodes	2 bands in the BPF 4 bands in the BSF	<0.92 dB	>26.5 dB	Not indicated
[7]	2.4 GHz	2 pin diodes	2	4.3 dB	38 dB	* $0.6\lambda_g \times 0.55\lambda_g$
[8]	1 GHz	2 pin diodes and 3 varactors	continuous	4.7 dB < IL < 5.6 dB	>13 dB	$0.14\lambda_g \times 0.12\lambda_g$
[9]	2.4 GHz	2 pin diodes	2	10 dB	30 dB	* $0.7\lambda_g \times 0.77\lambda_g$
[10]	1 GHz	2 pin diodes	2	* 1 dB	* 22 dB	$0.08\lambda_g \times 0.1\lambda_g$
This study	5 GHz	ScDDA	2	2.7 dB	>16 dB	$0.32\lambda_g \times 0.35\lambda_g$
This study	10 GHz	ScDDA	2	2.6 dB	>10 dB	$0.33\lambda_g \times 0.37\lambda_g$

* Estimated values from the figures.

6. Conclusions

In this paper, two reconfigurable bandpass filters were proposed and analyzed from synthesis to measurement. ScDDAs permit the commutation of the filter topology by a low bias voltage. Parasitic effects induced by classical active components are no longer a limitation to frequency increase. Moreover, the co-design method on an on-chip silicon substrate allows the integration of the active elements, reducing the overall size, manufacturing steps, and, consequently, the cost (in mass production). The demonstrators showed good performances, and the simulations fit the measurements well. The losses could be decreased with a higher substrate resistivity and higher doping amount, allowing resistivity in the junctions of around $0.1 \Omega \cdot \text{cm}$. Nevertheless, the demonstrators validate the approach and show advantages in design flexibility, integration, and cost.

Author Contributions: Conceptualization, R.A., F.L.B. and H.B.; methodology, R.A.; simulation and characterization, R.A.; validation, R.A., F.L.B., H.B., D.L.B. and C.Q.; manufacture, D.S.D.V., V.G., D.V. and J.B.; writing—original draft preparation, R.A.; writing—review and editing, F.L.B., H.B., D.L.B., C.Q. and D.S.D.V.; supervision, D.L.B., C.Q. and J.B. All authors have read and agreed to the published version of the manuscript.

Funding: This work was partly supported by both CERTeM Technological and RENATECH network French Platforms. This publication is also supported by the European Union through the European Regional Development Fund (ERDF), by the Ministry of Higher Education and Research and by Brest Métropole, Brittany, through the CPER Project SOPHIE/STIC & Ondes.

Data Availability Statement: Not applicable.

Conflicts of Interest: The authors declare no conflict of interest.

References

- Gentili, F.; Cacciamani, F.; Nocella, V.; Sorrentino, R.; Pelliccia, L. RF MEMS hairpin filter with three reconfigurable bandwidth states. In Proceedings of the 2013 European Microwave Conference, Nuremberg, Germany, 6–10 October 2013; pp. 802–805. [\[CrossRef\]](#)
- Bouyge, D.; Crunteanu, A.; Pothier, A.; Martin, P.O.; Blondy, P.; Velez, A.; Bonache, J.; Orlianges, J.C.; Martin, F. Reconfigurable 4 pole bandstop filter based on RF-MEMS-loaded split ring resonators. In Proceedings of the 2010 IEEE MTT-S International Microwave Symposium, Anaheim, CA, USA, 23–28 May 2010; pp. 588–591. [\[CrossRef\]](#)
- Blondy, P.; Palego, C.; Houssini, M.; Pothier, A.; Crunteanu, A. RF-MEMS Reconfigurable Filters on Low Loss Substrates for Flexible Front Ends. In Proceedings of the 2007 Asia-Pacific Microwave Conference, Bangkok, Thailand, 11–14 December 2007; pp. 1–3. [\[CrossRef\]](#)
- Araujo, L.d.; de Oliveira, A.J.B.; Llamas-Garro, I.; Mira, F.; Lancaster, M.J. Reconfigurable Microwave Coupled Resonator Band-pass Filter and Diplexer. In Proceedings of the 2019 SBMO/IEEE MTT-S International Microwave and Optoelectronics Conference (IMOC), Aveiro, Portugal, 10–14 November 2019; pp. 1–3. [\[CrossRef\]](#)

5. Cheng, T.; Tam, K. A Wideband Bandpass Filter With Reconfigurable Bandwidth Based on Cross-Shaped Resonator. *IEEE Microw. Wirel. Compon. Lett.* **2017**, *27*, 909–911. [[CrossRef](#)]
6. Simpson, D.J.; Gómez-García, R.; Psychogiou, D. Tunable Multiband Bandpass-to-Bandstop RF Filters. In Proceedings of the 2018 IEEE/MTT-S International Microwave Symposium-IMS, Philadelphia, PA, USA, 10–15 June 2018; pp. 1363–1366. [[CrossRef](#)]
7. Zahari, M.K.; Shairi, N.A.; Ahmad, B.H.; Zakaria, Z.; Wong, P.W. Miniaturized Switchable Bandpass to Matched Bandstop Filter Using Stepped-Impedance Resonator. In Proceedings of the 2018 IEEE International Workshop on Electromagnetics: Applications and Student Innovation Competition (iWEM), Nagoya, Japan, 29–31 August 2018; pp. 1–2. [[CrossRef](#)]
8. Song, K.; Chen, W.; Patience, S.R.; Chen, Y.; Iman, A.M.; Fan, Y. Compact Wide-Frequency Tunable Filter With Switchable Bandpass and Bandstop Frequency Response. *IEEE Access* **2019**, *7*, 47503–47508. [[CrossRef](#)]
9. Zahari, M.K.; Ahmad, B.H.; Wong, P.W.; Shairi, N.A. Switchable bandstop to bandpass filter using parallel-coupled resonator. In Proceedings of the 2017 IEEE Asia Pacific Microwave Conference (APMC), Kuala Lumpur, Malaysia, 13–16 November 2017; pp. 513–516. [[CrossRef](#)]
10. Kumar, N.; Singh, Y.K. Switchable compact widestopband bandstop filter to wideband bandpass filter. In Proceedings of the 2015 Asia-Pacific Microwave Conference (APMC), Nanjing, China, 6–9 December 2015; pp. 1–3. [[CrossRef](#)]
11. Zhu, H.-R.; Ning, X.-Y.; Huang, Z.-X.; Wu, X.-L. An Ultra-Compact On-Chip Reconfigurable Bandpass Filter With Semi-Lumped Topology by Using GaAs pHEMT Technology. *IEEE Access* **2020**, *8*, 31606–31613. [[CrossRef](#)]
12. Bergeras, F.; Duéme, P.; Plaze, J.; Darcel, L.; Jarry, B.; Campovecchio, M. Novel MMIC architectures for tunable microwave wideband active filters. In Proceedings of the 2010 IEEE MTT-S International Microwave Symposium, Anaheim, CA, USA, 23–28 May 2010; pp. 1356–1359. [[CrossRef](#)]
13. Shahid, I.; Thalakatuna, D.N.; Karmokar, D.K.; Mahon, S.J.; Heimlich, M. A Compact Reconfigurable 1-D Periodic Structure in GaAs MMIC With Stopband Switching, Dual-Band Operation and Tuning Capabilities. *IEEE Access* **2021**, *9*, 142084–142094. [[CrossRef](#)]
14. Allanic, R.; le Berre, D.; Quéré, Y.; Quendo, C.; Chouteau, D.; Grimal, V.; Valente, D.; Billoué, J. Three-State Microwave Tunable Resonator Integrating Several Active Elements on Silicon Technology in a Global Design. *IEEE Microw. Wirel. Compon. Lett.* **2018**, *28*, 141–143. [[CrossRef](#)]
15. Allanic, R.; le Berre, D.; Quéré, Y.; Quendo, C.; Chouteau, D.; Grimal, V.; Valente, D.; Billoué, J. Continuously Tunable Resonator Using a Novel Triangular Doped Area on a Silicon Substrate. *IEEE Microw. Wirel. Compon. Lett.* **2018**, *28*, 1095–1097. [[CrossRef](#)]
16. Allanic, R.; le Berre, D.; Quendo, C.; Chouteau, D.; Grimal, V.; Valente, D.; Billoué, J. A Novel Synthesis for Bandwidth Switchable Bandpass Filters Using Semi-Conductor Distributed Doped Areas. *IEEE Access* **2020**, *8*, 122599–122609. [[CrossRef](#)]
17. Allanic, R.; le Berre, D.; Quendo, C.; Chouteau, D.; Grimal, V.; Valente, D.; Billoué, J. Switchable DBR Filters Using Semiconductor Distributed Doped Areas (ScDDAs). *Electronics* **2020**, *9*, 2021. [[CrossRef](#)]
18. Allanic, R.; le Berre, D.; Quendo, C.; Chouteau, D.; Grimal, V.; Valente, D.; Billoué, J. Frequency Reconfigurable Interdigital Filter Using Semi-conductor Distributed Doped Areas. In Proceedings of the 2019 IEEE Asia-Pacific Microwave Conference (APMC), Singapore, 10–13 December 2019; pp. 974–976. [[CrossRef](#)]
19. Sanchez-Soriano, M.Á.; Torregrosa-Penalva, G.; Bronchalo, E. Compact Wideband Bandstop Filter With Four Transmission Zeros. *IEEE Microw. Wirel. Compon. Lett.* **2010**, *20*, 313–315. [[CrossRef](#)]
20. Feng, W.; Shang, Y.; Che, W.; Gómez-García, R.; Xue, Q. Multifunctional Reconfigurable Filter Using Transversal Signal-Interaction Concepts. *IEEE Microw. Wirel. Compon. Lett.* **2017**, *27*, 980–982. [[CrossRef](#)]
21. Matthaei, G.L.; Young, L.; Jones, E.M.T. *Microwave Filters, Impedance-Matching Networks, and Coupling Structures*; McGraw-Hill Book Company, Inc.: Norwood, MA, USA, 1964; Volume 1, ISBN 9780890060995.
22. Ponchak, G.E. RF Transmission Lines on Silicon Substrates. In Proceedings of the 1999 29th European Microwave Conference, Munich, Germany, 5–7 October 1999; pp. 158–161. [[CrossRef](#)]